Metal–Organic Motifs

International Edition: DOI: 10.1002/anie.201702589
German Edition: DOI: 10.1002/ange.201702589

Structural Transformation and Stabilization of Metal–Organic Motifs Induced by Halogen Doping

*Lei Xie, Chi Zhang, Yuanqi Ding, and Wei Xu**

Abstract: *The structural transformation of supramolecular nanostructures with constitutional diversity and adaptability by dynamic coordination chemistry would be of fundamental importance for potential applications in molecular switching devices. The role of halogen doping in the formation of elementary metal–organic motifs on surfaces has not been reported. Now, the 9-ethylguanine molecule (G) and Ni atom, as a model system, are used for the structural transformation and stabilization of metal–organic motifs induced by iodine doping on Au(111). The iodine atoms are homogeneously located at particular hydrogen-rich locations enclosed by G molecules by electrostatic interactions, which would be the key for such an unexpected stabilizing effect. The generality and robustness of this approach are demonstrated in different metal–organic systems (G/Fe) and also by chlorine and bromine.*

Supramolecular chemistry,[1] which relies on non-covalent interactions, has been widely employed as an appealing strategy for controllable fabrication of surface nanostructures.[2,3] Owing to the advantage of dynamic characteristics of non-covalent interactions, the transformation of supramolecular nanostructures with constitutional diversity and adaptability would be of fundamental importance for potential applications in molecular switching devices.[4,5] Among others, by virtue of coordination selectivity and diversity with respect to different metals,[6,7] various static metal–organic structures can be fabricated on the surface, and furthermore these structures could be responsive to metal/molecule stoichiometric ratios, coverage, and/or temperatures resulting in structural transformations via dynamic coordination chemistry.[8–13] In addition to the abovementioned intrinsic regulation factors (that is, constituent molecules and metals), the introduction of a third agent may offer another train of thought to obtain structural transformations.[14,15] It is well known that halogen doping is a widely utilized method in polymer chemistry to transform polyacetylene and polyaniline to conductive polymers.[16,17] For on-surface chemistry, iodine atoms usually act as byproducts of on-surface dehalogenative reactions[18–23] or can be trapped as guests in the self-assembled structures.[24] Very recently, the direct introduction of iodine onto metal surfaces under UHV conditions has been successfully achieved to decouple covalent networks from the surface as an intercalation.[25] However, to our knowledge, the influence of halogen atoms on the formation of elementary metal–organic coordination motifs on surfaces has not been reported so far. It is thus of general interest to introduce halogen atoms to metal–organic coordination systems and explore the potential role of halogens in affecting the surface nanostructures.

In this study, we choose the 9-ethylguanine (G) molecule and the transition-metal atom Ni as a model system because 1) the G molecule has two neighboring binding sites (that is, O6 and N7, see Scheme 1) for forming metal–organic coordination bonds; 2) the Ni atom is able to coordinate with both sites, which makes it possible for the formation of multiple metal–organic motifs on the surface; and 3) the ethyl group could help to ascertain the molecular chirality within the formed nanostructures. On this basis, iodine (I_2) is introduced onto the coordination system. Herein, from the interplay of high-resolution scanning tunneling microscopy (STM) imaging and density functional theory (DFT) calculations, we show that 1) co-deposition of G molecules and Ni atoms with different stoichiometric ratios on the Au(111) surface results in the formation of two typical nanostructures composed of G_3Ni_1 and G_2Ni_2 motifs, respectively, as depicted in Scheme 1. Moreover, reversible transformations between

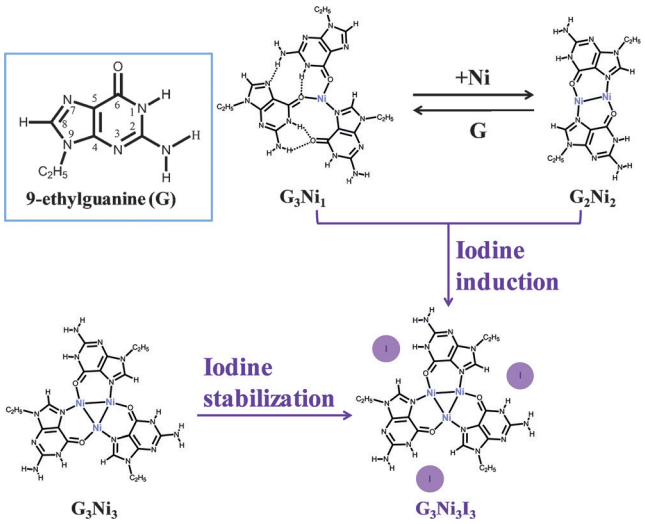

Scheme 1. Illustration of iodine-induced structural transformation and stabilization of elementary metal–organic motifs. Inset: chemical structure of the 9-ethylguanine molecule.

[*] L. Xie, C. Zhang, Y. Ding, Prof. Dr. W. Xu
Interdisciplinary Materials Research Center, Tongji-Aarhus Joint Research Center for Nanostructures and Functional Nanomaterials
College of Materials Science and Engineering, Tongji University
Shanghai 201804 (P.R. China)
E-mail: xuwei@tongji.edu.cn

Supporting information for this article can be found under: http://dx.doi.org/10.1002/anie.201702589.

these two structures are achieved in response to both G and Ni; 2) introduction of I_2 vapor to either of these two structures surprisingly induces the transformation to a different honeycomb structure composed of the $G_3Ni_3I_3$ motif where the iodine atoms are homogeneously located at specific hydrogen-rich harbors enclosed by G molecules via electrostatic interactions; 3) a control experiment demonstrates that introduction of I_2 vapor to the bare G_3Ni_3 structure (only formed under harsh conditions) also results in the formation of the $G_3Ni_3I_3$ structure and the existence of iodine atoms are found to be able to further stabilize the G_3Ni_3 structure; and 4) as a step forward, we have demonstrated the universality of this approach in regulation of metal–organic motifs by performing comparative studies with other coordination systems (for example, G/Fe), and other halogen atoms (namely, Cl, Br), which surprisingly result in characteristically the same honeycomb networks composed of the corresponding $G_3Fe_3I_3$, $G_3Ni_3Cl_3$ and $G_3Fe_3Br_3$ motifs, respectively. These experimental findings provide an example showing the role of halogen doping in facilitating the formation of specific elementary metal–organic coordination motifs on the surface.

Deposition of G molecules and Ni atoms (at a G/Ni ratio of ca. 4:1) on Au(111) at room temperature (RT) and further annealing at 390 K for 10 min results in the formation of a rhomboid network structure as shown in Figure 1a. From the close-up STM image (Figure 1b), we identify that the network structure is composed of two kinds of elementary motifs (that is, the trimeric and the dimeric ones as indicated by the corresponding contours). Two enantiomers of the trimeric motif are also observed as indicated by green and blue trimeric contours where the individual molecular chiralities are denoted by R and L. As experienced with coordination schemes between DNA bases and transition metals,[7,9,26–28] after extensive structural search, we assign this trimeric motif to a G_3Ni_1 metal–organic structure as highlighted in Figure 1c. From the DFT-optimized model superimposed on the corresponding STM image, we distinguish that it is formed by three G molecules (with different chiralities) coordinating with one Ni atom via one N7 site and two O6 sites, and the intermolecular NH···O and NH···N hydrogen bonds further stabilize the structure. The dimeric structure (depicted by the white contour in Figure 1b) is assigned to a hydrogen-bonded dimer according to the morphology and the well-established NH···O hydrogen bonds involved. These two elementary structural motifs are also linked together via hydrogen bonds.

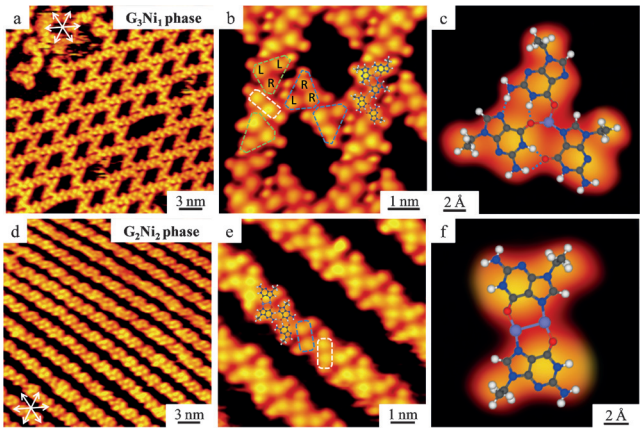

Figure 1. Formation of the rhomboid network and chain structure after deposition of G molecules and Ni atoms at a G/Ni ratio of ca. 4:1 and ca. 2:1 followed by further annealing at 390 K on Au(111). a) A large-scale STM image of the rhomboid network. b) A close-up STM image allowing us to identify the individual molecular chiralities (as indicated by L and R notations). The elementary G_3Ni_1 motifs with different chiralities are depicted by green and blue contours, respectively, and a G dimer is depicted by a white contour. c) High-resolution STM image of the G_3Ni_1 motif superimposed with the DFT-optimized model on Au(111); the substrate is omitted for clear presentation. d) A large-scale STM image of the chain structure. e) A close-up STM image allowing us to identify the elementary G_2Ni_2 motifs and G hydrogen-bonded dimers as depicted by the blue and white contours, respectively. f) High-resolution STM image of the G_2Ni_2 motif superimposed with the DFT-optimized model on Au(111); the substrate is omitted for clear presentation. Hydrogen bonds are depicted by blue dashed lines. H white, C gray, N blue, O red, Ni light blue.

By virtue of coordination diversity, deposition of G molecules and Ni atoms (at a G/Ni ratio of ca. 2:1) on Au(111) at RT and further annealing at 390 K for 10 min results in the formation of a chain structure as shown in Figure 1d. From the close-up STM image (Figure 1e), we identify that the chain structure is composed of two kinds of elementary motifs as depicted by the blue and white contours. Again, based on DFT calculations, we assign the dimeric motif in blue contour to a G_2Ni_2 metal–organic structure as highlighted in Figure 1f. From the DFT-optimized model superimposed on the corresponding STM image, we distinguish that it is formed by two homochiral G molecules coordinating with two Ni atoms via both N7 and O6 sites. The other dimeric structure (white contour) is the same hydrogen-bonded dimer as the one discussed above. These two elementary structural motifs are also linked together via hydrogen bonds. It is worth noting that the formation of such hybrid structures involving alternating metal–organic motifs and hydrogen-bonded dimers may be originated from the registry between metal–organic motifs with respect to the substrate lattice as reported previously.[9]

Furthermore, owing to the dynamic characteristics of coordination bonds, we have achieved reversible structural transformations between the above mentioned G_2Ni_2 and G_3Ni_1 motifs on Au(111) as shown in the Supporting Information, Figure S1 by adding G molecules or Ni atoms followed by annealing at 390 K for 10 min. Note that in the structural transformation processes we do not observe the formation of any other typical metal–organic motifs by changing either the G/Ni ratios or the post annealing temperatures. Furthermore, based on a thorough inspection of the obtained G_3Ni_1 and G_2Ni_2 structures, we find that the Au herringbone reconstruction remains intact indicating a weak interaction between metal–organic structures and surface (compare with the Supporting Information, Figure S2a).

To investigate the influence of halogen atoms on the formation of elementary metal–organic coordination motifs on the surface, we introduce I_2 into the system. After doping iodine (at a vapor pressure of ca. 10^{-7} mbar for 1 min) on either the G_3Ni_1 or G_2Ni_2 phase and further annealing such a sample at 490 K, interestingly, we observe the formation of

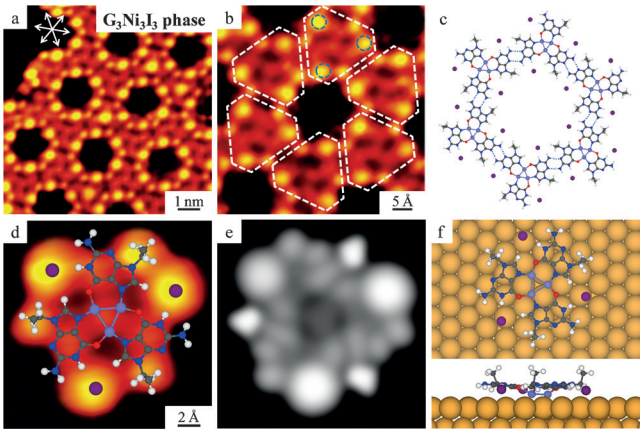

Figure 2. Formation of a typical honeycomb network structure composed of $G_3Ni_3I_3$ motifs after iodine doping on either the G_3Ni_1 or G_2Ni_2 phase and then annealing at 490 K on Au(111). a) A large-scale STM image of the honeycomb network. b) A close-up STM image allowing the identification of elementary $G_3Ni_3I_3$ motifs as depicted by the white contours in which the iodine atoms are indicated by the blue circles. c) The DFT-optimized gas-phase model of the hydrogen-bonded honeycomb network. d) The high-resolution STM image of the $G_3Ni_3I_3$ motif superimposed with the DFT-optimized model on Au(111). e) The simulated STM image of a $G_3Ni_3I_3$ motif. f) Top and side views of the relaxed model of $G_3Ni_3I_3$ motif on Au(111). H white, C gray, N blue, O red, Ni light blue, I purple.

a new honeycomb network structure as shown in Figure 2a. From the close-up STM image (Figure 2b), we identify that the honeycomb structure is composed of well-ordered elementary motifs as depicted by the white contours. As reported previously, I_2 would dissociate into atomic form and chemisorb on the surface under ultra high vacuum (UHV) conditions.[25] According to the previous findings[20,22,23] that halogen atoms are imaged as pronounced protrusions in STM images, we thus assign the bright spots indicated by the blue circles to iodine atoms. Moreover, the elementary motif also shows a protrusion in the center which is naturally assigned to metal. According to the restraints of molecular geometry ensured by the ethyl groups, both N7 and O6 sites of G molecules should coordinate with metal atoms and only a three-metal center could meet such a criterion as reported in previous literatures.[27–29] On this basis and further DFT calculations, we assign the elementary motif to a $G_3Ni_3I_3$ structure as highlighted in Figure 2d (see also the energetically most stable model on Au(111) in Figure 2f). From the DFT-optimized model, we distinguish that the motif is formed by three homochiral G molecules coordinating with three Ni atoms via both N7 and O6 sites, and three iodine atoms are located homogeneously at the specific hydrogen-rich harbors via electrostatic interactions.[24,30] The corresponding simulated STM image (Figure 2e) shows pronounced density of states of iodine atoms which is in a good agreement with the experimental image. These $G_3Ni_3I_3$ elementary motifs are then linked together by hydrogen bonds as shown in Figure 2c. Furthermore, a control experiment was performed by deposition of G molecules and Ni atoms (at a G/Ni ratio of ca. 1:1) and I_2 at the same time on the Au(111) surface at RT followed by further annealing at 390 K, which expectedly results in the same $G_3Ni_3I_3$ phase. It is also worth noting that the temperature applied to transform either the G_3Ni_1 or G_2Ni_2 phase to the $G_3Ni_3I_3$ one is higher than that of direct formation of $G_3Ni_3I_3$ phase (490 K vs. 390 K). Such a higher temperature is most probably required to desorb the excess G molecules from the surface to reach the G/Ni ratio of about 1:1 for the formation of $G_3Ni_3I_3$ phase, as pure G molecules desorb at 490 K. It is important to note that these findings show the first example where the halogens are found to be able to facilitate the formation of specific elementary metal–organic motifs on the surface, in which the particular adsorption sites for iodine atoms should be the key.

To further confirm the particular adsorption sites and explore the role of iodine atoms with respect to the specific metal–organic motifs, we tried to form the pure G_3Ni_3 phase by delicately controlling the growing process. After simultaneous codeposition of G and Ni (at a G/Ni ratio of ca. 1:1) on Au(111) held at a higher temperature of 430 K, interestingly we also observe the formation of another honeycomb network structure, as shown in Figure 3a. From the close-up STM image (Figure 3b), we identify that the honeycomb structure is composed of trimeric elementary motifs as depicted by the white contours. The three-metal center of the motif is also resolved as a spot protrusion. We thus assign this elementary motif to a G_3Ni_3 structure as highlighted in Figure 3c. The G_3Ni_3 motif has the same coordination pattern as that of $G_3Ni_3I_3$, and more importantly, it allows us to directly identify the iodine adsorption sites. The simulated STM image shown in Figure 3d is in a good agreement with the corresponding STM image. Note that the G_3Ni_3 phase can only be obtained in such a harsh condition mentioned above instead of general annealing procedures. The motif seems

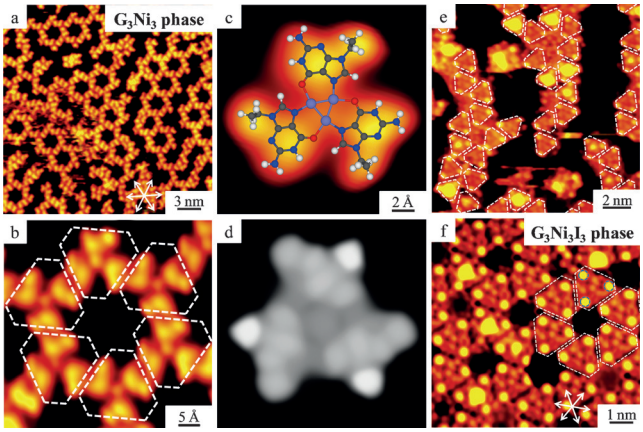

Figure 3. a)–d) Formation of another honeycomb network structure composed of pure G_3Ni_3 motifs after co-deposition of G and Ni simultaneously on Au(111) held at a high temperature of 430 K. a) A large-scale STM image of the G_3Ni_3 honeycomb network. b) A close-up STM image allowing the identification of elementary G_3Ni_3 motifs as depicted by the white contours. c) High-resolution STM image of the G_3Ni_3 motif superimposed with the DFT-optimized model on Au(111). d) Simulated STM image of a G_3Ni_3 motif. e) STM image after iodine doping on the G_3Ni_3-precovered surface at RT; the triangular motifs are depicted by white contours. f) Formation of the $G_3Ni_3I_3$ honeycomb network structure after annealing the surface at 370 K for 10 min; the $G_3Ni_3I_3$ elementary motifs are depicted by the white contours in which the iodine atoms are indicated by the blue circles.

unfavorable thermodynamically, and after further annealing at 370 K for 10 min, it turns to disarray.

To experimentally ascertain the iodine binding sites, we deposit I_2 onto the G_3Ni_3-precovered surface at RT, and find out that the Au reconstruction is slightly modified (Supporting Information, Figure S2b). A close-up image of the iodine-doped structure composed of triangular motifs is shown in Figure 3e. Further annealing the sample at 370 K for 10 min results in the same $G_3Ni_3I_3$ structure as shown in Figure 3f, where the herringbone reconstruction has been lifted which is clearly shown in a larger scale STM image as shown in the Supporting Information, Figure S2c. We thus unambiguously confirm that the iodine atoms prefer to bind at the hydrogen-rich harbors among G molecules. More interestingly, the $G_3Ni_3I_3$ phase can stand much higher temperature (ca. 490 K) than G_3Ni_3 (ca. 370 K) during thermal treatments, which indicates that the iodine doping not only facilitates the formation of the specific G_3Ni_3 metal–organic motif, but also stabilizes it in a lock-and-key mode. To provide an overview of these abovementioned four structures, a series of STM images in a larger scale are provided in the Supporting Information, Figure S3, which show good yields and represent the efficiency of the structure formation.

In a step forward, to explore the generality of the unexpected effect of iodine on regulating the formation of metal–organic motifs on the surface, we performed comparative studies to extend this approach to other coordination systems, and other halogen atoms (Cl, Br) are also investigated. As reported previously,[31] the G molecule and Fe atoms can form various metal–organic structures attributed to the dynamic characteristic of coordination bonds, while formation of the pure G_3Fe_3 network is rather difficult. Interestingly, when iodine is introduced to this system (at a G/Fe ratio of ca. 1:1) followed by annealing at 390 K for 10 min, we also observe the formation of a honeycomb network as shown in Figure 4a. From the close-up STM image (Figure 4b), we identify that the structure is composed of well-ordered elementary motifs as depicted by white contours. In comparison with the $G_3Ni_3I_3$ motif (compare Figure 2), we thus assign this motif to $G_3Fe_3I_3$.

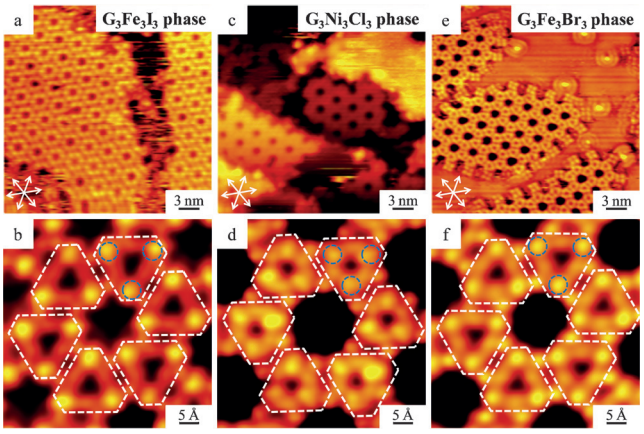

Figure 4. Large-scale and close-up STM images showing the $G_3Fe_3I_3$ (a, b), $G_3Ni_3Cl_3$ (c, d) and $G_3Fe_3Br_3$ (e, f) phases. The corresponding elementary motifs are depicted by white contours and the halogen atoms are indicated by blue circles.

To explore whether other halogens would play a similar role in regulation of metal–organic motifs, we tried to introduce Cl and Br atoms onto surfaces. As reported previously,[32] direct deposition of salts (like NaCl, KBr, $CaCl_2$) onto surfaces could serve as an alternative method to introduce both metal and halogen atoms. We just deposit the corresponding salts as $NiCl_2$ and $FeBr_2$ in the following experiments to construct metal–organic systems and dope halogens simultaneously. Deposition of G molecules and $NiCl_2$ on Au(111) followed by annealing at 390 K for 10 min also results in a characteristically the same honeycomb network as shown in Figure 4c, from the close-up STM image (Figure 4d), we assign the individual motif depicted by the white contour to $G_3Ni_3Cl_3$. Another control experiment has been carried out by deposition of G molecules and $FeBr_2$ on the surface followed by the same thermal treatment. Expectedly, a honeycomb network was observed (Figure 4e) and the individual motif (depicted by the white contour in Figure 4f) should be assigned to $G_3Fe_3Br_3$.

In conclusion, from a combination of submolecularly resolved STM imaging and DFT calculations, by employing different halogens and metal–organic systems, we therefore have demonstrated the generality and robustness of the unexpected effect of halogen atoms on regulating the formation of specific three-metal center coordination motifs on surfaces. These findings would make a step forward towards understanding the importance of halogen doping as a structure formation parameter, which provides a novel and universal strategy to controllable fabrication of surface nanostructures. In the future work, we attempt to investigate the influence of halogen doping effects on alkali and/or alkaline earth metal–organic structures to extend such a strategy to other systems.

Acknowledgements

The authors acknowledge financial supports from the National Natural Science Foundation of China (21473123, 21622307).

Conflict of interest

The authors declare no conflict of interest.

Keywords: halogen doping · metal–organic motifs · nickel · scanning tunneling microscopy · structural transformation

How to cite: *Angew. Chem. Int. Ed.* **2017**, *56*, 5077–5081
Angew. Chem. **2017**, *129*, 5159–5163

[1] J.-M. Lehn, *J. Inclusion Phenom.* **1988**, *6*, 351–396.
[2] T. Kudernac, S. Lei, J. A. A. W. Elemans, S. De Feyter, *Chem. Soc. Rev.* **2009**, *38*, 402–421.
[3] Y. Yang, C. Wang, *Chem. Soc. Rev.* **2009**, *38*, 2576–2589.
[4] F. P. Cometto, K. Kern, M. Lingenfelder, *ACS Nano* **2015**, *9*, 5544–5550.

[5] S.-L. Lee, Y. Fang, G. Velpula, F. P. Cometto, M. Lingenfelder, K. Müllen, K. S. Mali, S. De Feyter, *ACS Nano* **2015**, *9*, 11608 – 11617.
[6] A. Langner, S. L. Tait, N. Lin, R. Chandrasekar, V. Meded, K. Fink, M. Ruben, K. Kern, *Angew. Chem. Int. Ed.* **2012**, *51*, 4327 – 4331; *Angew. Chem.* **2012**, *124*, 4403 – 4407.
[7] L. Wang, H. Kong, C. Zhang, Q. Sun, L. Cai, Q. Tan, F. Besenbacher, W. Xu, *ACS Nano* **2014**, *8*, 11799 – 11805.
[8] D. Ecija, S. Vijayaraghavan, W. Auwärter, S. Joshi, K. Seufert, C. Aurisicchio, D. Bonifazi, J. V. Barth, *ACS Nano* **2012**, *6*, 4258 – 4265.
[9] H. Kong, C. Zhang, L. Xie, L. Wang, W. Xu, *Angew. Chem. Int. Ed.* **2016**, *55*, 7157 – 7160; *Angew. Chem.* **2016**, *128*, 7273 – 7276.
[10] J. Liu, T. Lin, Z. Shi, F. Xia, L. Dong, P. N. Liu, N. Lin, *J. Am. Chem. Soc.* **2011**, *133*, 18760 – 18766.
[11] A. Dmitriev, H. Spillmann, N. Lin, J. V. Barth, K. Kern, *Angew. Chem. Int. Ed.* **2003**, *42*, 2670 – 2673; *Angew. Chem.* **2003**, *115*, 2774 – 2777.
[12] M. Pivetta, G. E. Pacchioni, E. Fernandes, H. Brune, *J. Chem. Phys.* **2015**, *142*, 101928.
[13] T.-C. Tseng, N. Abdurakhmanova, S. Stepanow, K. Kern, *J. Phys. Chem. C* **2011**, *115*, 10211 – 10217.
[14] N. Lin, A. Langner, S. L. Tait, C. Rajadurai, M. Ruben, K. Kern, *Chem. Commun.* **2007**, 4860 – 4862.
[15] S. Lei, M. Surin, K. Tahara, J. Adisoejoso, R. Lazzaroni, Y. Tobe, S. De Feyter, *Nano Lett.* **2008**, *8*, 2541 – 2546.
[16] C. K. Chiang, C. R. Fincher, Y. W. Park, A. J. Heeger, H. Shirakawa, E. J. Louis, S. C. Gau, A. G. MacDiarmid, *Phys. Rev. Lett.* **1977**, *39*, 1098 – 1101.
[17] D. Kumar, R. C. Sharma, *Eur. Polym. J.* **1998**, *34*, 1053 – 1060.
[18] C. Zhang, Q. Sun, H. Chen, Q. Tan, W. Xu, *Chem. Commun.* **2015**, *51*, 495 – 498.
[19] Q. Fan, J. M. Gottfried, J. Zhu, *Acc. Chem. Res.* **2015**, *48*, 2484 – 2494.
[20] Q. Sun, L. Cai, H. Ma, C. Yuan, W. Xu, *ACS Nano* **2016**, *10*, 7023 – 7030.
[21] Q. Sun, L. Cai, H. Ma, C. Yuan, W. Xu, *Chem. Commun.* **2016**, *52*, 6009 – 6012.
[22] M. Bieri, et al., *J. Am. Chem. Soc.* **2010**, *132*, 16669 – 16676.
[23] L. Lafferentz, V. Eberhardt, C. Dri, C. Africh, G. Comelli, F. Esch, S. Hecht, L. Grill, *Nat. Chem.* **2012**, *4*, 215 – 220.
[24] T. Kaposi, et al., *ACS Nano* **2016**, *10*, 7665 – 7674.
[25] A. Rastgoo-Lahrood, et al., *Angew. Chem. Int. Ed.* **2016**, *55*, 7650 – 7654; *Angew. Chem.* **2016**, *128*, 7780 – 7784.
[26] H. Kong, Q. Sun, L. Wang, Q. Tan, C. Zhang, K. Sheng, W. Xu, *ACS Nano* **2014**, *8*, 1804 – 1808.
[27] H. Kong, L. Wang, Q. Sun, C. Zhang, Q. Tan, W. Xu, *Angew. Chem. Int. Ed.* **2015**, *54*, 6526 – 6530; *Angew. Chem.* **2015**, *127*, 6626 – 6630.
[28] H. Kong, L. Wang, Q. Tan, C. Zhang, Q. Sun, W. Xu, *Chem. Commun.* **2014**, *50*, 3242 – 3244.
[29] F. Bebensee, K. Svane, C. Bombis, F. Masini, S. Klyatskaya, F. Besenbacher, M. Ruben, B. Hammer, T. R. Linderoth, *Angew. Chem. Int. Ed.* **2014**, *53*, 12955 – 12959; *Angew. Chem.* **2014**, *126*, 13169 – 13173.
[30] B. E. Hirsch, K. P. Mcdonald, B. Qiao, A. H. Flood, S. L. Tait, *ACS Nano* **2014**, *8*, 10858 – 10869.
[31] C. Zhang, L. Wang, L. Xie, Y. Ding, W. Xu, *Chem. Eur. J.* **2017**, *23*, 2356 – 2362.
[32] C. Zhang, L. Wang, L. Xie, H. Kong, Q. Tan, L. Cai, Q. Sun, W. Xu, *ChemPhysChem* **2015**, *16*, 2099 – 2105.

Manuscript received: March 12, 2017
Final Article published: April 5, 2017

